An Investigation into Artificial Vortex Generation and Effects on Inlet Flow Quality Using Scaled Turbofan Engine Simulators

Undergraduate Honors Thesis

Presented in Partial Fulfillment of the Requirements for the Bachelor of Science with Research Distinction in the Undergraduate School of The Ohio State University

By

Gregory D. Rhodes

Undergraduate Program in Aeronautical and Astronautical Engineering

The Ohio State University

Professor Clifford A. Whitfield, Advisor

Professor Richard J. Freuler, Advisor

Jacob T. Allenstein. Co-Advisor

Department of Mechanical and Aerospace Engineering

April 2016

ABSTRACT

Jet engine inlet vortices have a tendency to form when the engine is stationary and operating at high thrust settings, such as during warmup and takeoff. A vortex will attach itself to the ground and extend upwards into the fan of the engine. This greatly increases the likelihood of damage to the engine fan and numerous internal components due to ingestion of foreign object debris (FOD) into the engine or engine vibration, which can directly lead to catastrophic engine failure. Naturally occurring vortices are extremely unsteady and unpredictable, making them particularly difficult to study. In order to study these vortices in a more efficient and inexpensive manner, an artificial vortex generator was designed and built. The vortex generator was designed to effectively and consistently imitate a naturally occurring vortex by adding swirl to previously established axial airflow via tangential air injection. This generator was placed on an artificial ground plane beneath an Ejector Powered System (EPS) type engine simulator to simulate an engine free-field environment. After visual confirmation of vortex formation, total and static pressures across the inlet of the engine simulator measured pressure fluctuations during the ingestion of the artificial vortex. The inlet distortion caused by the artificial vortex generator was comparable to the distortion expected to be seen by a naturally occurring vortex. Further analysis into inlet vortex effects on static pressure inside the engine bellmouth yielded lower static pressures due to increased velocity in the boundary layer as compared to a free field engine run.

The vortex generator was able to provide the necessary ambient vorticity required for a vortex to form. Investigating the nature by which an inlet vortex adversely affects jet engines plays a crucial role in jet engine inlet research and design. The following research will provide a strong foundation in the ability to consistently ingest a vortex into the engine, allowing for more efficient studies in how to mitigate vortex induced complications.

Dedicated to Mom and Dad

ACKNOWLEDGEMENTS

I would like to express my sincere gratitude to my advisors Dr. Whitfield and Dr. Freuler for their assistance and guidance throughout this project. They have dedicated their time and effort to better me as both a student and as an engineer, and for that I am deeply grateful. I would like to thank Mr. Jacob Allenstein and Mr. Kegan Buchhop for their help in the experimental setup and data acquisition.

I would like to extend my appreciation to the staff in the machine shop at the Aeronautical and Astronautical Research Laboratory at The Ohio State University, specifically Josh Gueth and Ken Fout. Their assistance in both designing and machining the vortex generator prototypes was immeasurable.

To the Department of Aeronautical and Astronautical Engineering at Ohio State, thank you for the opportunity to conduct research at the ARC and providing funding along the way.

Thank you to my father for generously donating experimental equipment for this research project.

Finally, I would like to thank my best friend Mr. Shane Raber for his support and encouragement both in and out of the classroom. I could not have asked for a better friend these last five years.

Table of Contents

List of Figures

List of Tables

Nomenclature

Symbol

A	Area
D	Diameter
H	Engine Centerline Height
$\dot{m}$	Mass Flow
$\overline{m}$	Mass Fraction
M	Mach Number
P	Static Pressure
P_o	Total Pressure
R	Specific Gas Constant (Air)
SP	Sensitivity or Error of Parameter
T	Temperature
Uη	Uncertainty of Precision Limits
V	Velocity
γ	Ratio of Specific Heats (Air)
ρ	Density

Subscripts

e	Exit / Exhaust Plane
i	Inlet Plane
o	Total Conditions
x	Arbitrary Axial Distance from Exhaust Plane
∞	Freestream Conditions

Abbreviations

ARC	Aerospace Research Center
EPS	Ejector Powered System
FOD	Foreign Object Debris
ID	Inlet Distortion
JETS	Jet Engine Test Simulation
PSI	Pounds per Square Inch
PSIA	Pounds per Square Inch Absolute

PSID	Pounds per Square Inch Differential
SAE	Society of Automotive Engineers

Chapter I:
Introduction

1.1 Background

When a jet engine is in high thrust operation near a ground plane in static or near static conditions, such as the beginning of takeoff, an inlet vortex can form, anchoring to the ground and extending into the engine inlet. On a very fundamental level, a jet engine inlet vortex is the rotation of air about a common, centerline axis. This phenomenon is unsteady and difficult to predict its location and strength. In the case of operating a turbofan or turbojet engine near ground level at a high thrust setting, the engine is ingesting a significant mass flow through the inlet. A vortex of air could form from the ground and extend upwards into the fan face. As the vortex nears the entrance to the engine inlet, the flow accelerates and the rotational velocity increases, causing the vortex diameter to decrease. The high velocity in the core of the vortex causes the lowest pressure in the flow, and the pressure increases as one moves away from the core, in accordance with Bernoulli's Principle. Once formed, the vortex can move, stretch, and twist [1]. Because the core of the vortex is of extremely low pressure, if the dew point is sufficient, the water vapor in the air can condense and the core of the vortex will become visible. This effect can be seen below in Figure 1.

Figure 1: Visible Vortex due to Condensate in Core [2]

The motivation for this research will be immediately followed by a brief explanation as to how the vortices naturally form. Additionally, previous vortex research methods will be described and the chapter will conclude with the purpose of the current research.

1.1.1 Research Motivation

As previously mentioned, the static pressure at the center of the vortex is significantly lower than the surrounding atmospheric pressure. Therefore, it has the ability to pick up foreign object debris (FOD) from the runway or taxiway and ingest it directly into the engine, likely damaging the fan and various other internal components. In normal operation with the absence of a vortex, Trapp et al. has estimated that the average suction force induced by the engine inlet flow is less than one pound. However, the introduction of an inlet vortex has been estimated to increase this suction force to nearly 40 pounds [2].

Furthermore, a jet engine inlet vortex can cause severe fan blade vibrational effects. As a fan blade comes into contact with the low pressure center, the blade is being pushed forward into the core of the vortex from the higher pressure air on the aft side of the blade. If the vibrations match that of the fan blades' natural frequency a catastrophic failure can occur. Even without a full blade failure, vibrational effects are known to contribute to high cyclic fatigue [3]. Consequently, the life of each fan blade is significantly reduced and would have to be replaced sooner, which imposes a larger expense for the operator.

Finally, if a vortex is ingested into the core of the engine, the compressor has a potential to stall. A stall in a jet engine is the disruption of the airflow in the compressor. A compressor stall, depending on severity, can result in a momentary drop in power to a complete loss of compression, which in turn will result in more fuel consumption. For all of these reasons it is important to understand how these vortices form and the impacts they can have on engine performance.

1.1.2 Vortex Formation

Previous studies have identified that three criteria must be met in order for a vortex to naturally form [4]. First, there must be a stagnation point. Naturally, there will be omnidirectional flowing air parallel to the ground surface to which the vortex would be anchored. The flows must converge at a single point on the ground where the net velocity of the flow is zero. Such conditions are often modeled as a sink in fluid dynamics. Second, there must be an updraft. The jet engine provides this updraft as it ingests air adjacent to the ground plane into the fan. The third and final condition required for a ground vortex to form is ambient vorticity. A crosswind would be able to provide this vorticity. It should be noted that these are

proposed necessary but not sufficient conditions for vortex formation. Figure 2 illustrates how these three conditions assemble to form a ground vortex.

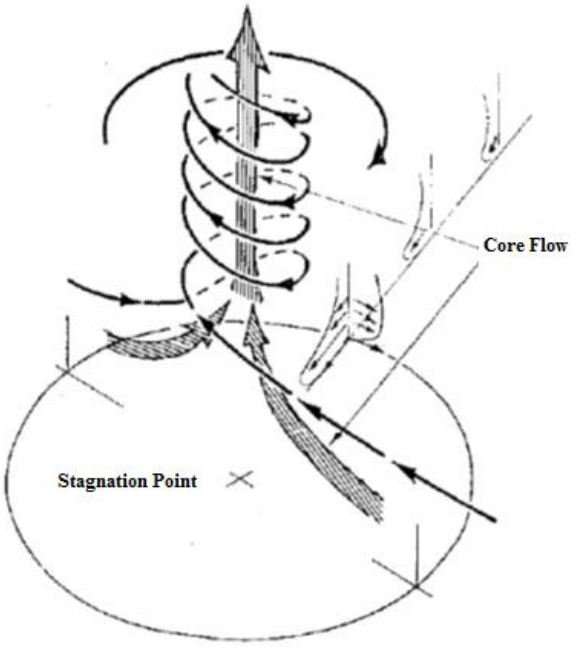

Figure 2: Necessary Conditions for Vortex Formation [5]

When studying vortices in this environment, four distinct parameters are commonly used: engine centerline height (H), wind velocity/ambient vorticity (V_o), engine inlet velocity (V_i), and engine inlet diameter (D_i) [5]. These variables are labeled below in Figure 3.

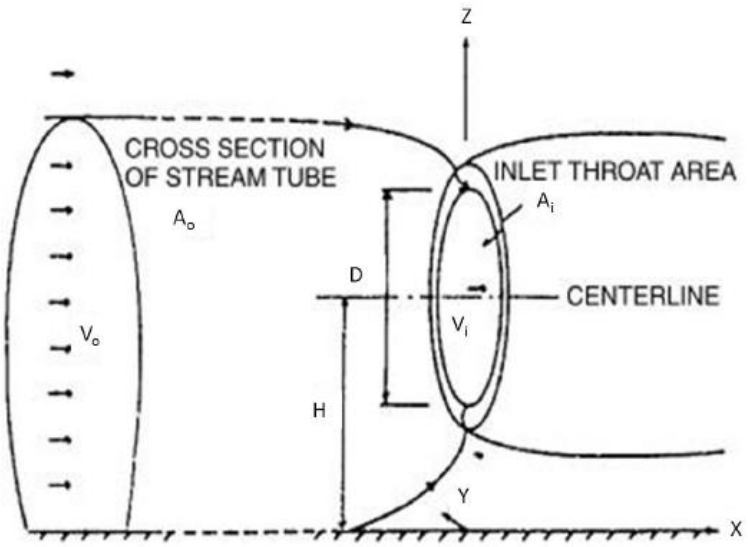

Figure 3: Common Parameters in Vortex Ingestion Analysis [2]

A second set of conditions suggested for a ground vortex to form is very similar to the previously mentioned criteria. Again, a non-zero ambient vorticity must be present. In addition to the vorticity, the centerline of the engine and the ground plane must be sufficiently close together, and the velocity beneath the engine must be less than that of the blow-away velocity. Blow-away velocity is the speed at which a vortex can no longer form without being completely removed by the oncoming flow. The volume of air in front of the engine that is directly affected by the engine while in operation is known as the stream tube, which has a cross-sectional area of A_o. If the engine centerline becomes sufficiently low enough, the stream tube and the ground plane will intersect. The intersection of these two planes induces a ground velocity, and combined with a crosswind or ambient vorticity, a vortex has the potential to form.

Researchers Horvath and Ho, among others, have used the non-dimensional velocity ratio ($\frac{V_i}{V_o}$) and the length ratio ($\frac{H}{D_i}$) to help predict when a vortex is likely to form. Several different studies of a turbofan engine in a free field environment, shown in Figure 4, have plotted this

velocity ratio against the length ratio. A line was drawn that divides when a vortex is and is not expected to form.

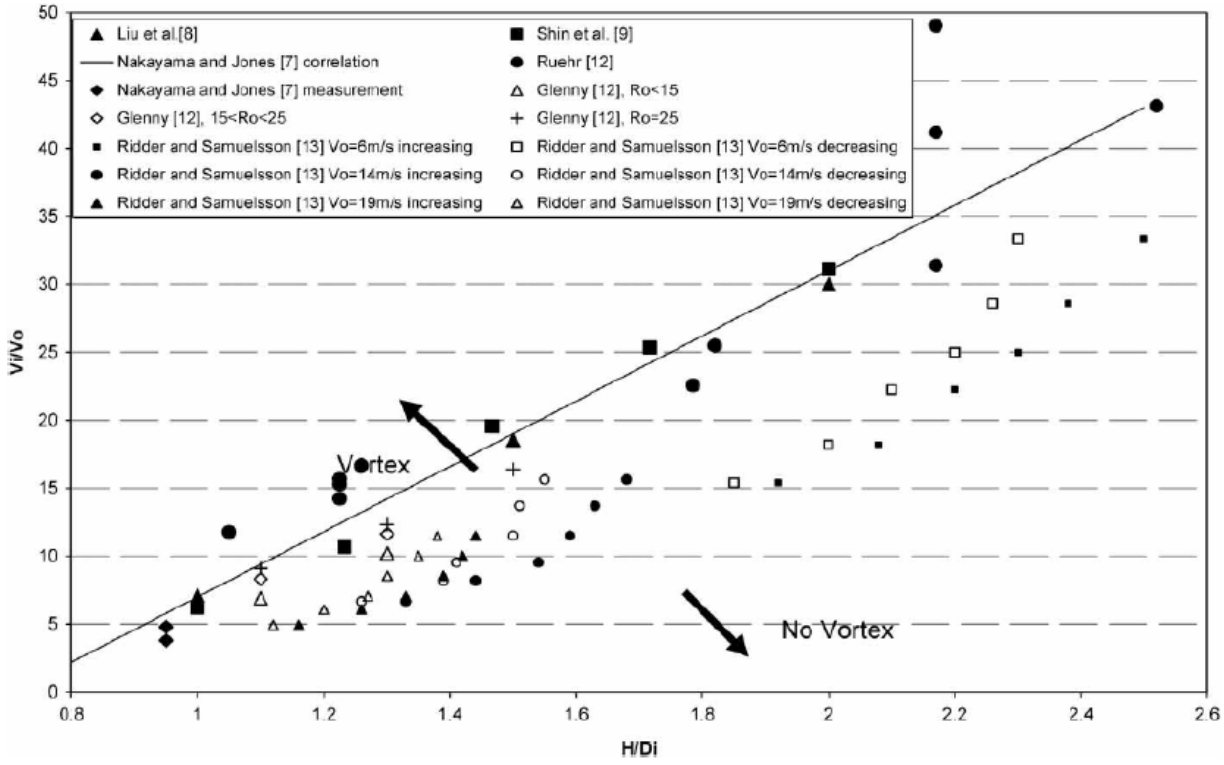

Figure 4: Experimental Vortex Prediction Data [6]

With any given engine mounted configuration, the distance from the ground to the centerline of the engine (H) and the inner diameter of the engine (D_i) are fixed values. Figure 4 allows engineers to analyze the likelihood that a vortex will form at any given length ratio. It should be noted that the line drawn may not always hold true due to a phenomenon known as hysteresis. Once a vortex is formed, it may remain standing despite the V_i dropping low enough to put the ratio into the "No Vortex" section of Figure 4.

1.1.3 Previous Vortex Study Techniques

Studying the effects of vortices on jet engine performance is quite difficult. A vortex is unsteady and unpredictable. If a vortex is formed in a laboratory setting, the airflow disturbance induced by a person walking on the other side of the room can be enough of a disruption for the vortex to completely dissipate.

Some studies have tried to replicate vortex flow using passive techniques. A passive technique is one in which the vortex would be a by-product of some other phenomenon. In contrast, an active approach would manipulate flow in such a way to directly reproduce a vortex. A study by NASA in 1975 studied the effect of inlet ingestion of a wing tip vortex on compressor face flow and turbojet stall margin. A wing was placed inside of a wind tunnel such that when air passed over the top, a vortex was formed by the pressure differential on either side of the wing. An engine downstream of the wing intercepted and ingested the vortex [7].

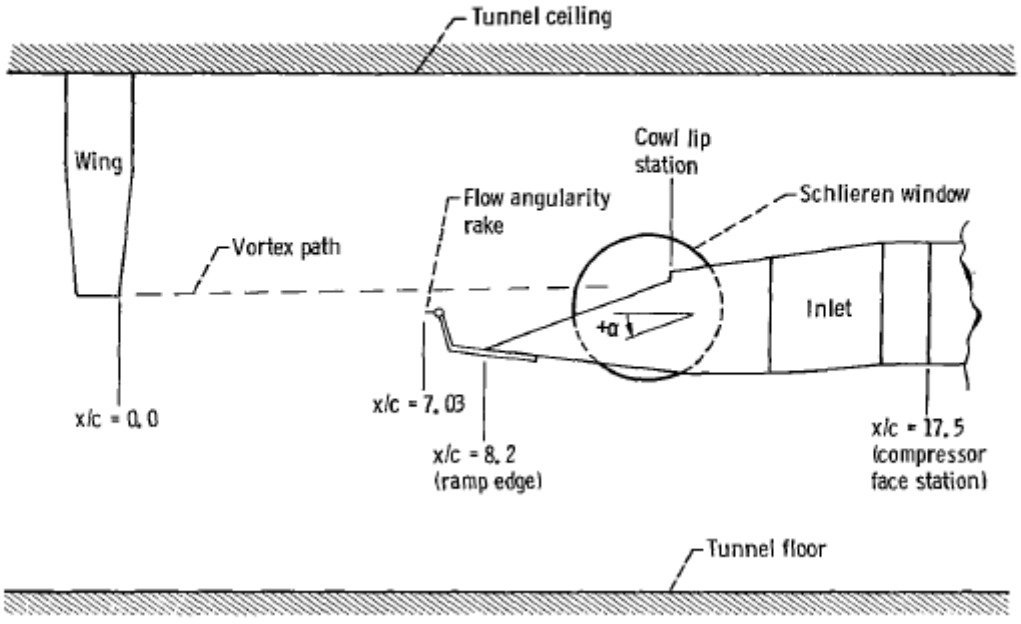

Figure 5: Passive Vortex Generator [7]

For this research, a wingtip vortex is undesirable. These vortices are much larger than a ground vortex and will have different properties and effects on the engine. Moreover, it is desirable to have more control over the vorticity or tangential velocities of the vortex. This would be very difficult to control in a passive technique.

1.2 Purpose of Current Research

The present research aims to design, fabricate, and validate an artificial vortex generator. Validation of the generator required that the inlet distortion caused by the vortex generator be comparable to the distortion expected to be encountered with a naturally occurring vortex. The generator was designed such that it could be mounted directly underneath an artificial ground plane with the resultant vortex being ingested directly by a jet engine simulator. A computer-aided design (CAD) program was utilized to aid in the drawing and designing prior to fabrication. The generator was designed such that the tangential and axial velocities could be controlled independently. Once built, confirmation of vortex generation was accomplished visually. After visual confirmation, an engine simulator was run to simulate takeoff conditions overtop the functioning generator. In this configuration, pressure fluctuations were recorded in order to compare the inlet distortion caused by the vortex generator and the distortion seen by a naturally occurring vortex.

Finally, measurements were taken in order to examine how the static pressure conditions inside the engine inlet are affected. The process in which the vortex generator was built and validated is described in greater detail in Chapter III. Research results and conclusions will follow in Chapter IV and V, respectively.

Chapter II:
Facility, Equipment, and Experimental Setup

2.1 Experimental Facility

All experimentation was performed at The Ohio State University's Aerospace Research Center (ARC) in Columbus, Ohio. This facility was able to provide the highly pressurized air necessary to run ejector-powered engine simulators, which will be further discussed in this chapter. Furthermore, this facility has been studying the aerodynamics of engine simulators for over 30 years and provides a strong foundation on which the current research can build upon.

2.2 Engine Simulators

A thorough understanding of how an engine simulator operates is extremely important in order to obtain reliable data during experimentation. The engine simulators used in this research were of the Ejector Powered System type, or EPS-type simulator. High pressure air is exhausted through multiple ejector nozzles inside the simulator. The benefit of EPS-type simulators is that there are no moving parts, making this type of simulator the preferred choice when studying potentially dangerous phenomena such as vortices. These types of simulators can be broken down into four distinct sections: the engine inlet, engine exhaust, air supply/ejectors, and a mixing zone. Figure 6 below illustrates a cross-section of this type of simulator with these components clearly labeled.

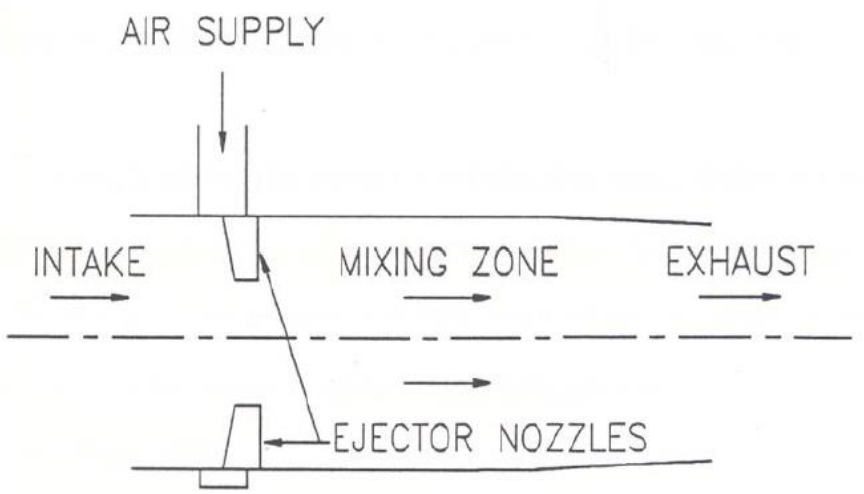

Figure 6: Cross-Section of Ejector-Powered Engine Simulator [8]

In order to accurately represent the performance of a full scale engine, the model must maintain four characteristics: engine geometry, inlet and exhaust mass flow rates, and exhaust plane thrust (momentum) [9]. Inconsistencies in these characteristics will result in the loss of a direct correlation in performance between the engine simulator and the full scale engine.

The ejectors dictate the performance of the simulator. As seen in Figure 7 they are placed at equal spacing peripherally around the inside of the model to not only produce a uniform flow, but also help match the exhaust flow conditions and thrust produced by the full-scale engine.

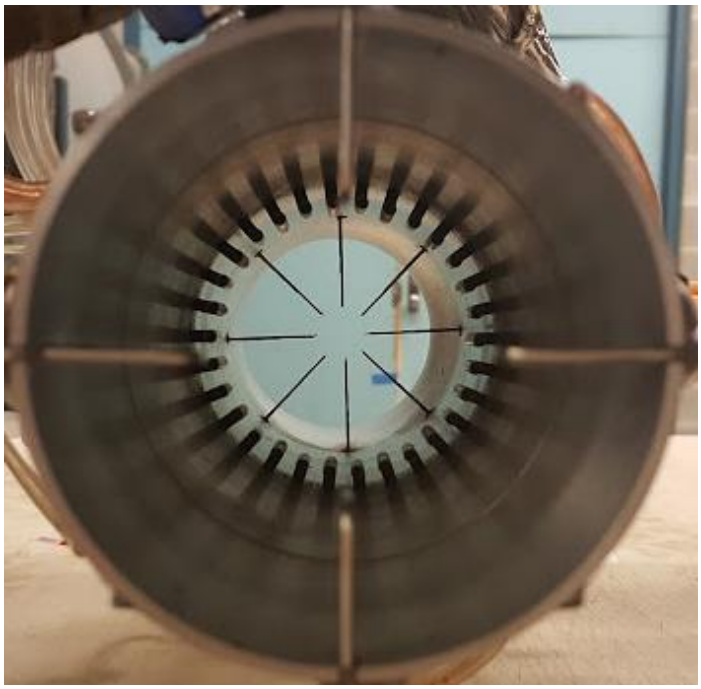

Figure 7: Ejectors in an EPS-type Engine Simulator

In order to calculate the aerodynamic thrust produced, the following equation derived from the law of conservation of momentum can be used:

$$Thrust = A_e[(P_e - P_\infty) + \rho_e V_e^2] \tag{2.1}$$

Using the total and static pressure ports along with the thermocouple located at the aft end of the simulator, the total mass flow through the engine can be calculated. Mass flow ($\dot{m}$) is defined as:

$$\dot{m} = \rho_e V_e A_e \tag{2.2}$$

Combining Equations (2.1) and (2.2), the aerodynamic thrust equation becomes:

$$Thrust_x = A_x \rho_x V_x^2 = \dot{m} V_x = \dot{m} M_x \sqrt{\gamma R T_x} \tag{2.3}$$

where the subscript *x* denotes any x-location located downstream of the exit plane. An important note to make on Equation (2.3) is that if all other variables were kept constant, the mass flow through the simulator would need to be increased over that of the scaled full-scale engine by a factor of the square root of the ratio of the temperatures in order to accurately match the thrust produced by the full-scale engine [8] The necessary increase in mass flow through the simulator is supplied by the ejectors located inside. It is this precise principle that forms the fundamental design of ejector-type engine simulators [8].

2.2.1 Representative 2000 Pound Thrust Class Engine

The EPS engine simulator utilized in this research was a one-sixth scale model of a commercial turbofan engine capable of producing 2,000 pounds of thrust full scale. Pressurized air was ejected through 30 supersonic ejectors, each one-sixth inches in diameter located circumferentially around the inside wall of the simulator at a 12° separation as seen in Figure 7. The pressurized air came from two, 2,300 PSI-rated air storage tanks located at the ARC. The air was routed from these tanks to a manual regulator, allowing for variable supply pressures. The regulator was directly connected to the engine via a vertical strut on which the engine hung, as seen in Figure 8. The strut could be moved vertically inside the thrust stand to allow the engine centerline height from the artificial ground plane to be adjusted.

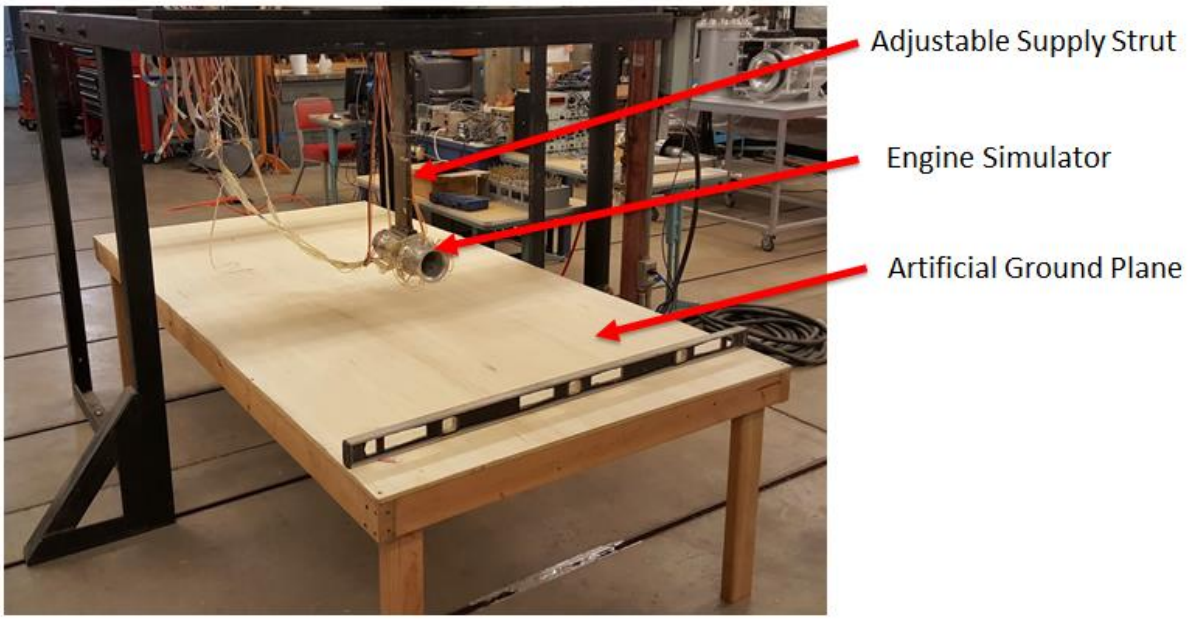

Figure 8: Engine Simulator and Artificial Ground Plane

The engine has the capability of being fitted with either a bellmouth inlet or a flight cowl. A bellmouth inlet allows for uniform inlet flow under static engine testing conditions, whereas a flight cowl is designed specifically for flight conditions. As a result, the flight cowl often causes a non-uniformity in engine inlet flow under static conditions. The bellmouth was used in order to better "capture" a vortex. Because a bellmouth produces a uniform flow, any changes in pressure (indicating the presence of a vortex) can be more easily observed.

The bellmouth and the flight cowl have fan inlet and exit diameters of 2.9 and 2.8 inches, respectively. Inside the inlet are eight total pressure rakes forward of the fan station each with five immersions for a total of 40 total pressure ports. Each rake is separated equally by 45°. Between each total pressure rake is a static pressure port. These pressure ports are used to measure pressure distribution across the inlet plane.

Located at the engine exhaust plane are four total pressure rakes. There are four total probes on these rakes for a total of 16 total pressure readings. These rakes are separated equally by 90°.

There are also four static ports located halfway between each exhaust pressure rake. The total pressure measurements at the exhaust plane can be used in conjunction with the static pressure measurements in order to calculate the aerodynamic thrust of the engine.

2.3 Experimental Setup

In order to obtain the most accurate results, a static, wind-free environment is ideal. The introduction of a crosswind can disturb the inlet flow of the engine. A free-field test stand was set up inside the Jet Engine Testing Simulation (JETS) laboratory at the ARC. This type of stand allows the engine to run without experiencing airflow disruption caused by neighboring objects. The ambient vorticity required for a vortex to form was provided by the vortex generator, which will be discussed in Chapter III. An artificial ground plane was built in order house the vortex generator. The ground plane was designed to be large enough such that turbulent flow induced from the edge of the ground plane would not be ingested into the engine inlet and disrupt the investigations.

The engine simulator was placed on a vertical strut in which the pressurized supply air traveled through to reach the engine simulator ejectors. The vertical strut was clamped to a mounting block that was free to pivot about a single axis such that thrust measurements could be made. Figure 8 illustrates the engine in the free field test stand with the artificial ground plane [10].

Directly underneath the centerline of the engine, a hole was cut in the artificial ground plane equal to the outer diameter of the vortex generator. As seen in Figure 9 the vortex generator was then mounted underneath the ground plane such that the exit was flush with the ground plane. A regulator was mounted on the side of the ground plane and connected to compressed shop air with a total available pressure of 75 PSI. The regulator allowed for the axial and tangential

supply pressures of the vortex generator to be controlled individually. An aerial view looking down towards the ground plane can be seen in Figure 10.

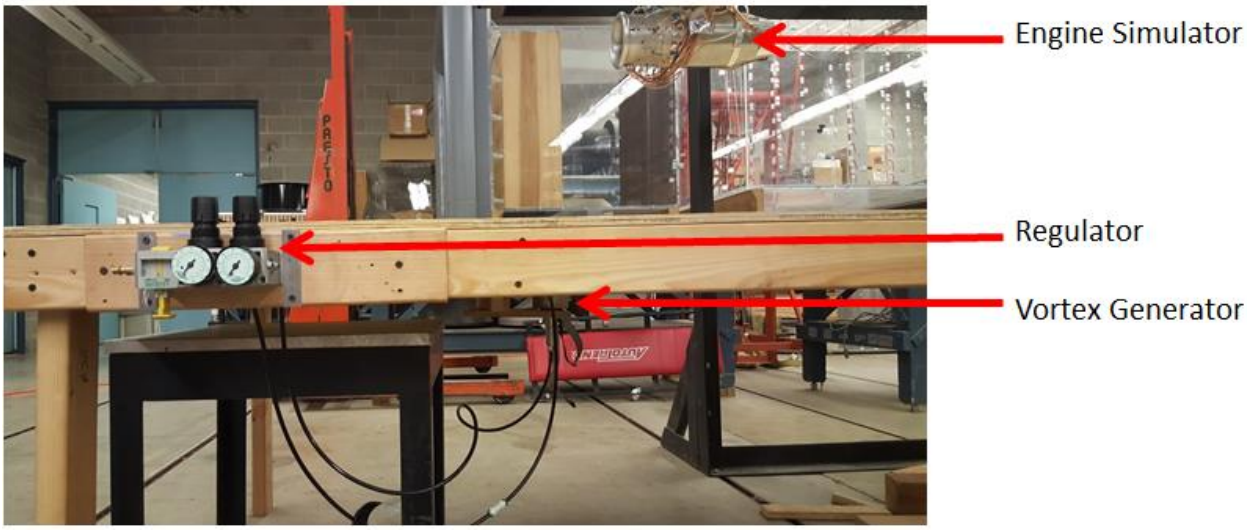

Figure 9: Engine Simulator with Vortex Generator

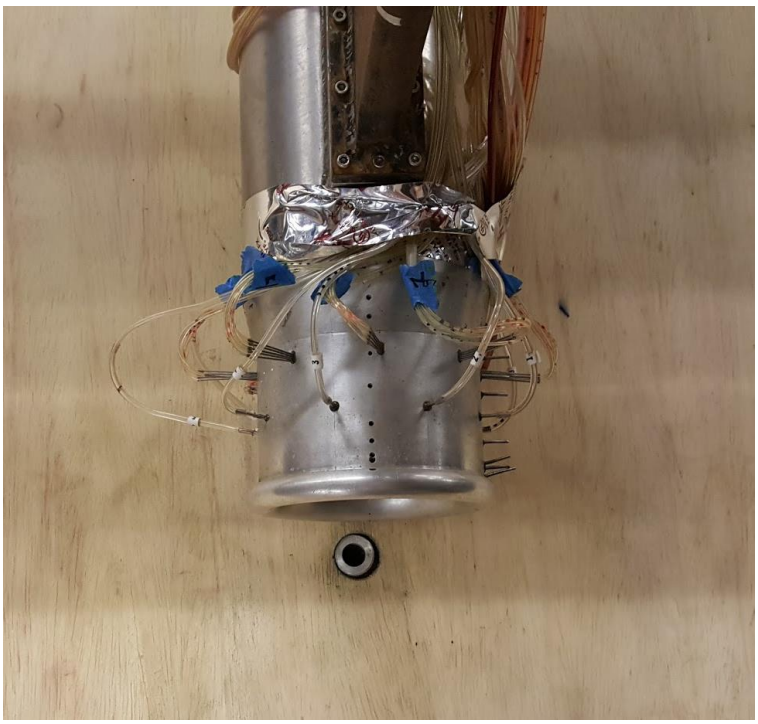

Figure 10: Engine Simulator above Vortex Generator Exit

2.4 Experimental Equipment

Equipment was needed to collect the pressure and temperature measurements. The ARC Jet Engine Test Simulation (JETS) laboratory supplied the necessary instrumentation for this research. The following section describes the exact equipment that was utilized in this research.

2.4.1 Pressure Measurements

The 2,000 pound thrust equivalent full-scale engine simulator operated in this experiment is fitted with pressure measurement instrumentation in both the bellmouth and the exhaust. The pressure ports for both static and total pressures connected directly to six individual pressure scanners via plastic tubing. Each of these Measure Specialties pressure scanners were fitted with 16 pressure transducers. The transducers, as seen in Figure 11, ranged from one PSID up to 15 PSID.

Figure 11: Pressure Scanner (background) and Pressure Transducers [8]

The pressure differential is with respect to the reference pressure, in this case ambient pressure. The differential pressure inside the bellmouth of the engine is expected to be quite low. Therefore, the one PSID transducer was used for this location. With a small pressure differential, a low PSID rated transducer is desirable for more accurate data as the accuracy is a function of the transducer's full scale output. Each pressure scanner was connected to a NetScanner 90DB Distribution Box. In addition to supplying the necessary electrical power to the pressure scanners, the distribution box also relays the signals from the scanners back to the computer via Ethernet connection.

Figure 12: NetScanner 90DB Distribution Box [9]

2.4.2 Temperatures

Temperature measurements were recorded in three different locations during the experiment: ambient conditions, engine exhaust, and inside the air supply line (just downstream of the manual regulator). The temperatures were collected with an Omega Type T Thermocouple that is composed of a copper-constantan alloy. Each thermocouple was connected to a National

Instruments SCXI-1102 Thermocouple/Voltage Input Module to relay the readings to the computer. Figure 13 below shows the thermocouple at the aft of the engine simulator.

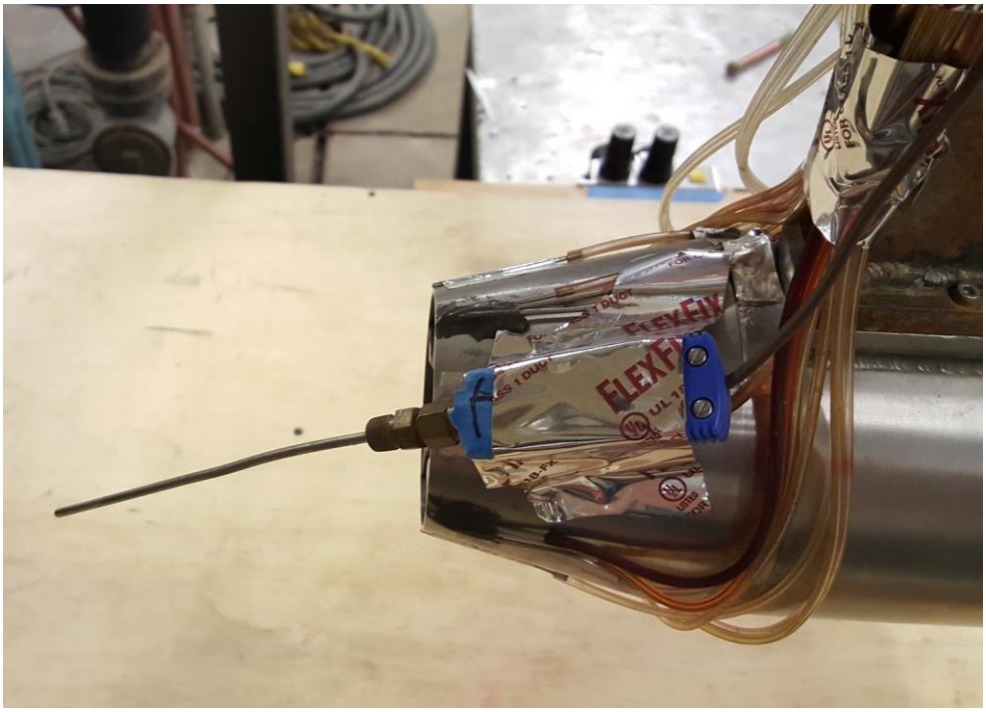

Figure 13: Thermocouple near Aft End of Engine Simulator

2.4.3 Air Supply

The compressed air used to drive the engine simulator was supplied by the two aforementioned 2,300 PSI supply tanks. The air from these tanks was routed to a central control location inside the laboratory. At this location the manual regulator, connected to a pressure gauge, could be opened and closed accordingly until the desired operating drive pressure was obtained. In conjunction with the pressure gauge, the pressure was monitored with a Validyne differential pressure transducer (DP-15). The differential pressure transducer is connected to a

Validyne Carrier Demodulator signal conditioning unit (CD-15) which feeds the voltage to the computer. A barometer inside the lab was used to obtain an accurate ambient pressure reading. A summary of the equipment used and their respective specifications and accuracies can be seen in Table 1.

Table 1: Specifications of Equipment [9]

Temperature

- OMEGA Quick Disconnect Molded, Copper-Constantan Thermocouple (Type T)
- Temperature Range: -454 to 752 °F (-270 to 400 °C)
- Error: Temperature > 32°F is 0.75% F.S

Pressure

- Measurement Specialties Pressure Scanner NetScanner System 9116
- Range: 1 PSID, 2.5 PSID, 5 PSID, 10 PSID and 15 PSID
- Pressure Inputs per Scanner: 16
- Static Accuracy (after Rezero): ± 0.05 % F.S. for transducers > 2.5 PSID
    - ± 0.15 % F.S. for transducers < 2.5 PSID

- Validyne Engineering DP15 Variable Reluctance Differential Pressure Transducer
- Range: 1250 psi
- Accuracy: ± 0.25% Full Scale
- Output: ± 35 mv/V Full Scale Output

Chapter III:
Vortex Generator Design

3.1 Vortex Generator

The overall design goal for the vortex generator was to provide operational simplicity while developing consistent conditions conducive to vortex formation. Several different configurations were considered that utilized lessons-learned from previous designs, including past projects at the ARC. One such project focused on developing and controlling inlet flow swirl conditions for an engine simulator that was designed for air-breathing marine and industrial power generation applications.

A drawing of the final vortex generator design can be seen in Figure 14. Many of the dimensions, such as inlet and outlet diameters, overall length, and number of holes drilled are somewhat arbitrary. The device was constructed with simplicity in mind.

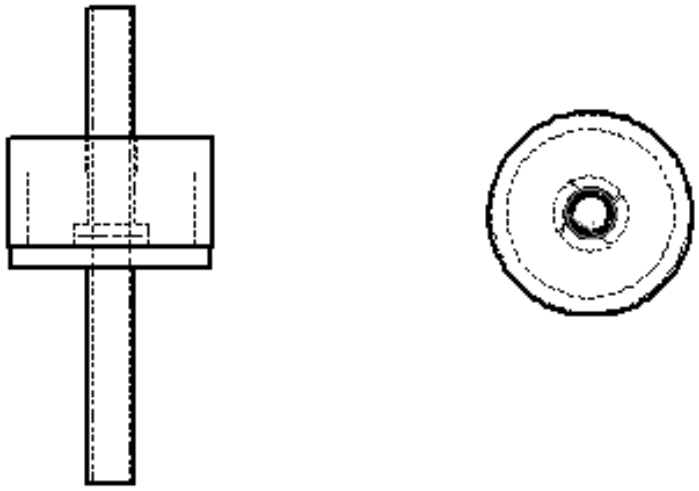

Figure 14: Drawing of Vortex Generator

The vortex generator is divided into two sections: the axial tube and the plenum chamber. A piece of aluminum tubing (0.5 inch inner diameter, 0.875 inch outside diameter) was used for the axial tube. Aluminum was the material of choice because, in addition to being readily available, it is easier to work with and a soft metal to machine. Near the midpoint of the tube, four small holes were drilled such that each hole was approximately tangential to the inside diameter. Consequentially, the air exiting through these holes forces the previously established axially flow to rotate.

A larger and hollowed out cylinder lay overtop these holes, forming a plenum chamber. The chamber was sealed to the axial tube approximately one inch on either side of the holes. A 0.25 inch quick-connect fitting was fitted to this plenum chamber. The quick-connect fitting was routed to one side of the regulator via plastic tubing. When the valve in the regulator is opened, air is allowed to flow directly into the chamber. The chamber quickly becomes pressurized and air is forced through the small holes into the interior of the axial tube.

A second quick-connect fitting was threaded into one end of the axial tube. This fitting was also connected via plastic tubing to the second of two valves in the regulator system. The regulator had a single input (shop air) and two independently controlled exits. This allowed the pressure supplied to the axial flow to be controlled independently from the plenum chamber. When the vortex generator is in full operation with both regulator valves open, air flows directly into the axial tube. When it reaches halfway up the tube, the pressurized air from the plenum chamber is forced into the axial stream, causing it to rotate. The now rotating fluid continues downstream and exits into ambient conditions. A cross-sectional view of the vortex generator illustrating the directional flow of the air can be seen below in Figure 15. Figure 16 depicts a top-

down view of the vortex generator, illustrating how the air from the pressure plenum enters tangentially into the axial flow. The arrows inside the vortex generator indicate the movement of the air. Note that the vortex generator itself is completely stationary. Only the fluid inside is rotating. The actual vortex generator used in experimentation can be seen in Figure 17.

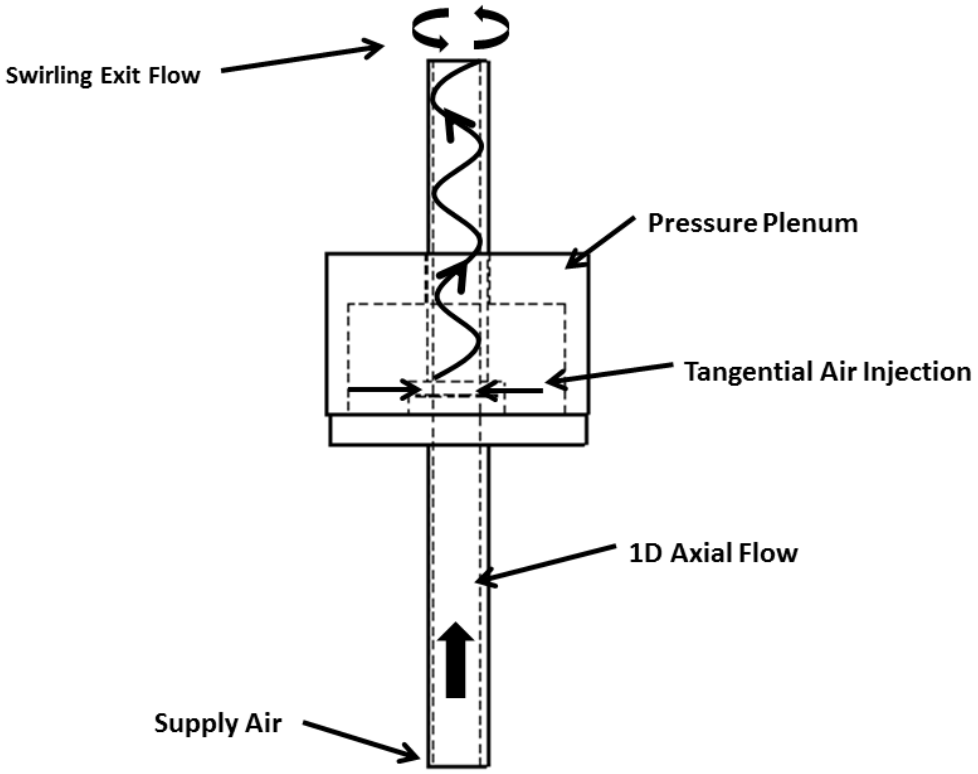

Figure 15: Cross-Sectional View of Vortex Generator

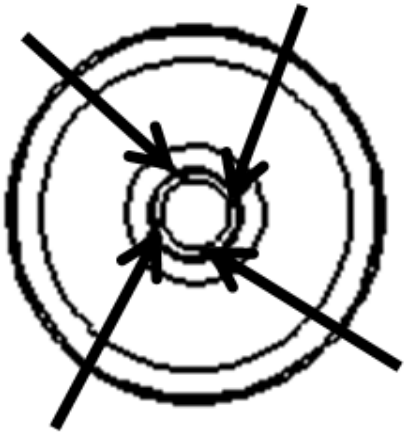

Figure 16: Top View of Vortex Generator

Figure 17: Vortex Generator Used in Experimentation

Before experimentation continued, a very simple flow visualization technique was performed to ensure that the exiting air was in fact rotating and not just highly turbulent flow. After the vortex generator was securely mounted to the underside of the artificial ground plane, the axial pressure was set to a small value while the plenum remained unpressurized. A small piece of yarn attached to the end of a short aluminum rod was placed into the flow. As expected, the yarn was blown directly upwards and held perpendicular to the artificial ground plane. While the yarn was still being held vertical, the pressure inside the plenum was slowly increased. Immediately the yarn began to rotate slowly in a circular pattern. This visualization setup can be seen in Figure 18. With this verification of rotating fluid, experimentation continued to attempt the reproduction of a naturally occurring vortex.

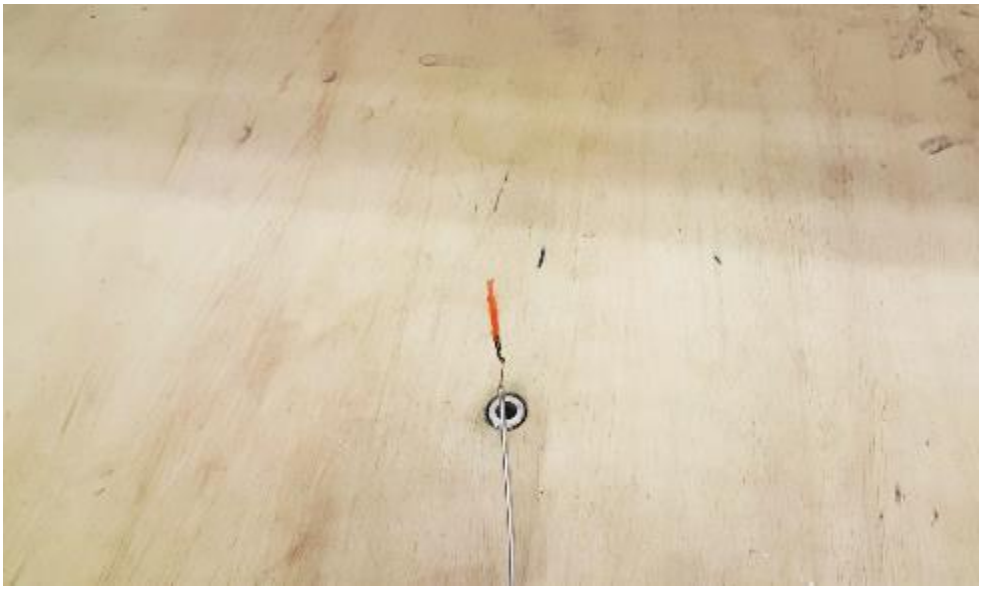

Figure 18: Flow Visualization Technique

3.2 Data Acquisition

A central computer was used to process all data. The computer runs Windows XP 32 bit and included a National Instruments SCXI-1102 Thermocouple/Voltage Input Module and a National Instruments BNC/TC-2095. Voltage inputs from the thermocouples and pressure transducers previously mentioned in Chapter II are processed by these two modules. Data was acquired using LabVIEW 11.0. The program allows the user to perform calculations and monitor the performance of the engine simulator in real time.

3.3 Measurement Validity

Each of the six Measurement Specialties pressure scanners contained 16 transducers for a total of 96 pressure transducers. As seen from Table 1, each of the transducers under 2.5 PSID has a static accuracy of 0.05% full scale and 0.15% full scale for all others. The temperature readings in this study were obtained using an Omega Thermocouple, which has an accuracy of ± 1.5 % corresponding to ± 0.015 of the recorded values at temperatures greater than 32 degrees Fahrenheit. These temperature readings in combination with the pressure readings were used in

determining the aerodynamic thrust of the engine. The accuracies of the instrumentation measurements were used to determine the uncertainty values expected with engine simulator performance characteristics. The analysis is provided in the following section.

3.3.1 Measurement Uncertainty Analysis

An uncertainty analysis regarding experimental measurements was conducted in order to understand the total experimental equipment error associated with the system. The total error is composed of both bias and precision error. Bias error is the constant error associated with a given system. This is the error most closely related to the accuracy of the measurements. Precision error is the difference between experimental values under unchanged testing conditions. An uncertainty analysis is designed to bound the accuracy of the collected data. Measurement uncertainty analysis provides investigators with test validation, helps identify the corrective action needed to achieve their test objective(s), helps reduce errors, and helps stay in compliance with agreements and contracts [9].

The calculated aerodynamic thrust of the engine simulator required data from both the pressure scanner and thermocouple from the exhaust plane. These pressure transducers are rated to 15 PSID with an accuracy of 0.015% full scale. This bounds the result to ± 0.023 PSID. If the assumption that the accuracy is linear throughout the range of the transducer, and neglecting bias, the following equation can be applied [11]:

$$U_\eta = \left[\left(S_{P_1}\right)^2 + \left(S_{P_2}\right)^2 + \ldots + \left(S_{P_N}\right)^2 \right]^{1/2} \tag{3.1}$$

where $S_{P_1}$is the sensitivity of parameter 1 up to N parameters. The result U is the uncertainty of the precision limits. For example, if Equation 3.1 is applied to the pressure transducer and thermocouple accuracies, the aerodynamic thrust calculation has an uncertainty of:

$$U_\eta = [\,(0.15)^2 + (1.5)^2]^{1/2} = 1.51 \tag{3.2}$$

Equation 3.2 above shows that the total uncertainty in the calculated aerodynamic thrust as given by LabVIEW has an accuracy of ± 1.51 percent. Thus, the aerodynamic thrust uncertainty is given by Equation 3.3

$$\text{Aerodynamic Thrust Uncertainty} = \pm\,(0.0151) \cdot \text{Aerodynamic Thrust} \tag{3.3}$$

3.4 Data Reduction

After each run of the engine simulator, the LabVIEW code produces a Microsoft Excel spreadsheet with the calculated pressure values, thrust values, and other performance parameters. The transducers take sample readings at 500 Hz over a five second timespan and the value provided in the spreadsheet is the average of these values. A MATLAB script file was written to read in the inlet pressure values and map them across the face of the bellmouth

3.5 Free Field Testing

Several engine runs were performed in a free field, static environment. No artificial ground plane or vortex generator was present. This was done to verify that all pressure transducers were working properly. The pressure values recorded by each transducer can be seen in the Microsoft Excel file that is generated after each run. If one of the pressures was significantly different than

the majority of the other pressure values (by a factor of 10) then a troubleshooting process would begin. A hole in the tubing connecting the port and the transducer could cause a bad reading as the tube would be losing pressure. The tube could also be clogged with debris the engine had ingested, blocking the total pressure from the transducer. If after the troubleshooting process the transducer was still reading significantly different values, that transducer would be labeled faulty and not considered in the calculations. Seen below in Figure 19 is a representation of the locations of the inlet total pressure locations in the standard convention of aft looking forward (ALF), looking upstream at the flow entering the engine simulator.

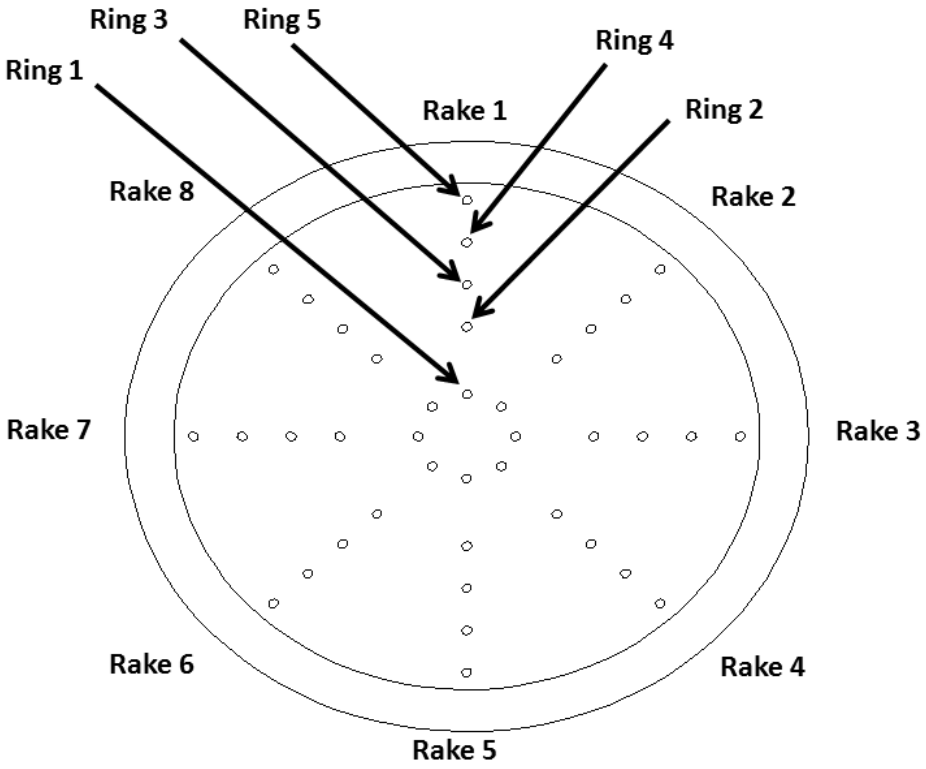

Figure 19: Total Pressure Rake and Port Locations (ALF)

Figure 20 shows the distribution of pressure over the inlet of the engine simulator under full thrust, free field, and static conditions. Using MATLAB, a shading technique was implemented in order to interpolate pressure values between rings. The inlet of the engine is commonly

referred to as “plane seven” or P7. When referring to a specific pressure, the rake is identified using “PT”, and the ring is identified using “RG”. For example, ring one on rake one at the engine inlet would be referred to as P7PT1RG1.

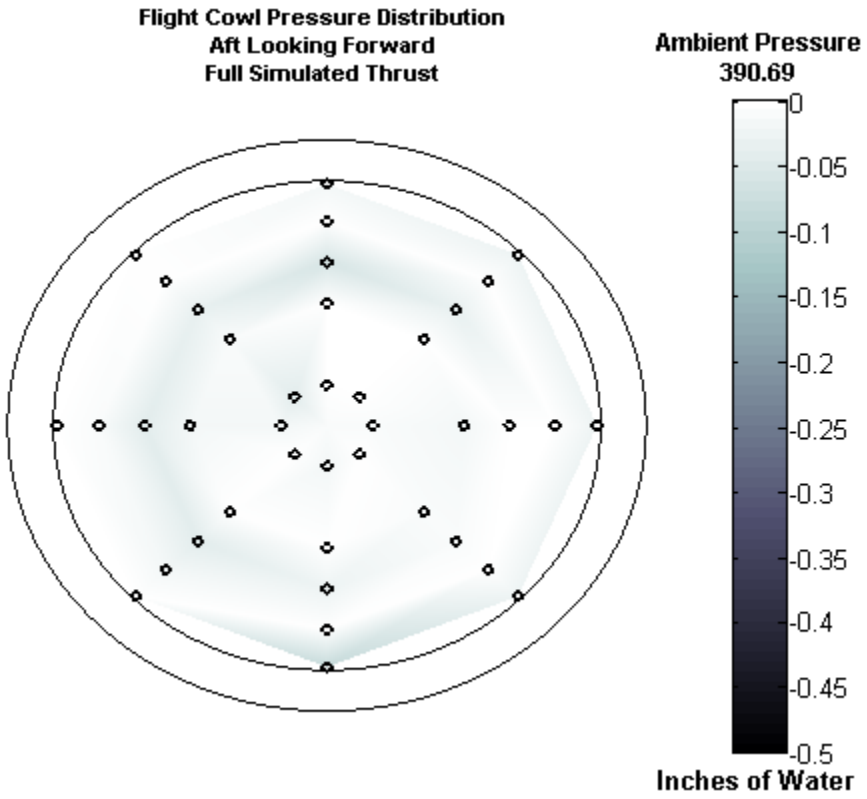

Figure 20: Engine Inlet in Free Field Static Test at Simulated Full Thrust

The total inlet distortion corresponding to this run is 0.02% overall total pressure variation. Inlet distortion is a metric used to characterize the quality of inlet flow in the inlet of an engine. The Society of Automobile Engineering (SAE) Aerospace Recommended Practice (ARP1420B) states the inlet distortion should be less than 0.30% total pressure variation. This ARP provides guidelines by which gas turbine engine aerodynamic stability and performance, as affected by the quality of the airflow delivered to the engine, can be evaluated consistently. Inlet distortion can be calculated using Equation 3.4 [12].

$$ID = \frac{(P_{max} - P_{min})}{P_{avg}} \tag{3.4}$$

where P is the total pressure measured at the fan face. Because 0.02 is much less than 0.30, a value of 0.02% was considered acceptable. Once the bellmouth was found to accurately display the pressure distribution across the front of the engine, the experiment could proceed on to visually confirming vortex generation.

3.6 Vortex-Engine Mass Flow Fraction

Due to the lack of equipment capable of measuring the vorticity or velocity components inside the vortex, the strength of the vortex generated was not able to be precisely quantified. However, it was possible to correlate the mass flow through the engine simulator to the mass flow exiting the vortex generator. This ratio, or the mass flow fraction, creates a relationship between the vortex and the engine simulator.

As mentioned previously, the vortex chamber can be divided into two main components: the axial tube and the pressure plenum. The total mass flow exiting the vortex generator is the sum of the mass flow coming from each of these components. The pressure supplied to each component is the total pressure in the system. The static pressure can be approximated using the local ambient conditions. Using Equation 3.5, the Mach number can be calculated for each system using these two pressure values and assuming a ratio of specific heats equal to 1.4.

$$\frac{P_o}{P} = \left(1 + \frac{\gamma - 1}{2} M^2\right)^{\frac{\gamma}{\gamma - 1}} \tag{3.5}$$

The ambient density can be calculated using Equation 3.6, where ambient conditions were used for the pressure and temperature.

$$\rho = \frac{P}{RT} \tag{3.6}$$

The mass flow can then be calculated using the flowing equation:

$$\dot{m} = \rho VA = \rho M\sqrt{\gamma RT}A \tag{3.7}$$

where the area is either the area of the opening in axial tube or the area of the small holes inside the pressure plenum, depending on which mass flow is desired. By adding the mass flows of these two components, an overall mass flow exiting the generator can be calculated, which will be referred to as $\dot{m}_{v.}$

The mass flow through the simulator is already calculated in the Microsoft Excel sheet provided as discussed in section 3.4. This mass flow is designated $\dot{m}_{sim.}$ The mass flow fraction can then be found by taking the ratio of these two values:

$$\overline{m} = \frac{\dot{m}_{sim}}{\dot{m}_{v}} \tag{3.8}$$

In this research, it should be noted the pressure plenum was kept at a constant pressure of 40 PSIG. Therefore, the swirl component remained constant and any change in $\dot{m}_v$ was strictly due to changes in supply pressure to the axial tube.

3.7 Vortex Visualization

The first objective while running the engine was to observe the vortex formed by the vortex generator. A commercially available smoke machine was setup near the inlet of the engine. A converging nozzle was machined to receive the smoke from a large diameter and eject it through small diameter. This was done in order to inject the smoke in precisely the desired location. In addition to the smoke, an LED light was altered such that the light could only escape through a small slit. The slit produced a small curtain of light, and the laboratory lights were shut off to improve lighting conditions.

Figure 21: Vortex Visualization Setup

Seen above in Figure 21 is the visualization setup. The light curtain produced by the LED lights is in the background. The airflow into the engine can easily be seen due to the added smoke from the smoke machine.

In order to obtain the best photo of the vortex, the experiment was video recorded and then viewed frame by frame. After several recordings, a vortex was finally captured. The vortex can be seen below in Figure 22 . This run had the engine running at simulated full thrust, corresponding to a mass fraction of approximately 6.64.

Figure 22: Artificial Vortex Visualization

With this visual confirmation of vortex formation, the first phase of the research purpose has been successfully completed. The next step of the research could then proceed, where the effects of the vortex on the engine inlet pressure distribution would be studied. The vortex ingested results will be discussed in Chapter IV.

3.8 Engine Simulator and Vortex Ingestion

After vortex visualization, the vortex generator was confirmed to have the capability of reproducing a naturally occurring vortex. The next step was to run the generator and the engine simulator simultaneous and study the effects the vortex had on the engine simulator. For all engine runs, the H/D_i ratio was fixed at approximately 1.5. With this ratio, the engine centerline was 4.5 inches from the ground plane. All experimentation was conducted with the engine operating at full simulated takeoff thrust, as vortex ingestion commonly occurs at high thrust static conditions The pressure in the plenum remained constant and the pressure supplied to the axial tube was varied throughout the experiment.

Chapter IV:
Ingested Vortex Results and Discussions

4.1 Total Pressure Results at Engine Inlet

The engine simulator was run with the vortex generator operating in order to capture how the pressure inside the fan face was affected by the presence of a vortex.

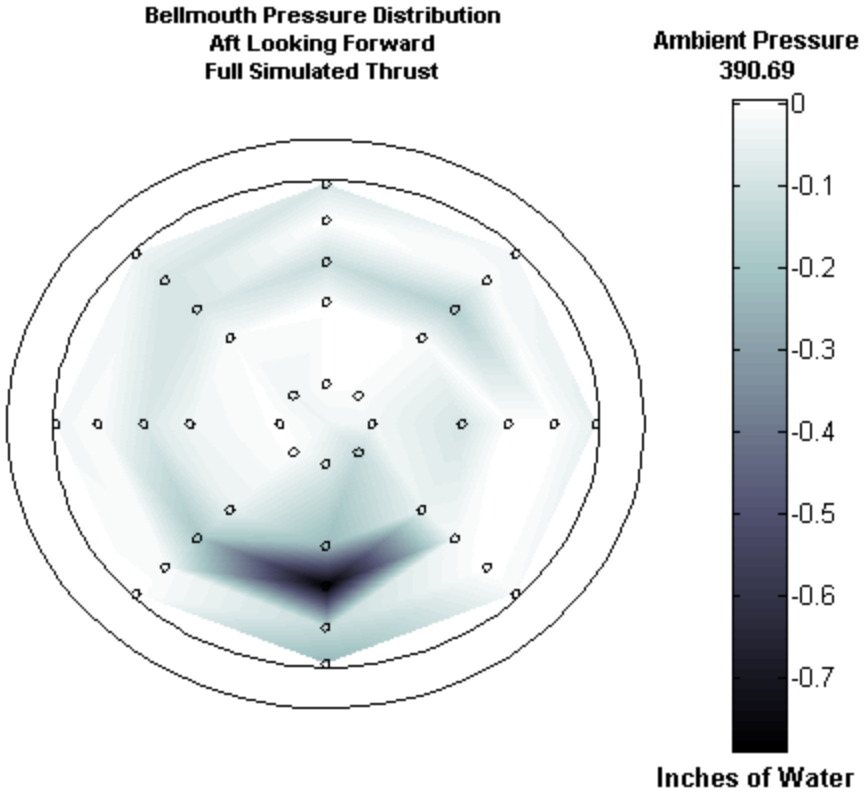

Figure 23: Artificial Vortex Capture

An example of the distribution of pressure inside the engine inlet during vortex ingestion can be seen above in Figure 23. In this run, the mass fraction was 6.82 and the overall bellmouth distortion was 0.22%. The location of the vortex is represented in the blue, precisely on P7PT5RG3 where the pressure drops to approximately 0.7 inches of water below ambient. It is important to note that this area of low pressure is not necessarily the location of the core of the

vortex. A vortex, as stated before, is unsteady and unpredictable in its movement. When the vortex is arbitrarily close to one of these total pressure ports, the low pressure in the core will influence the pressure surrounding it. Therefore, the vortex seen in Figure 23 is likely just near enough P7PT5RG3 to see the effects it has on that precise location. Seen below is Figure 24, where the engine was run at exactly the same mass fraction as the figure above. However, although the inlet looks very similar to the distortion seen above in Figure 23, the overall bellmouth distortion in this run was only 0.10% overall. The magnitude of the pressure drop induced by the vortex is higher in the inlet seen above. This is to say that the vortex generated above was more near this probe and thus had a greater influence (causing lower pressure).

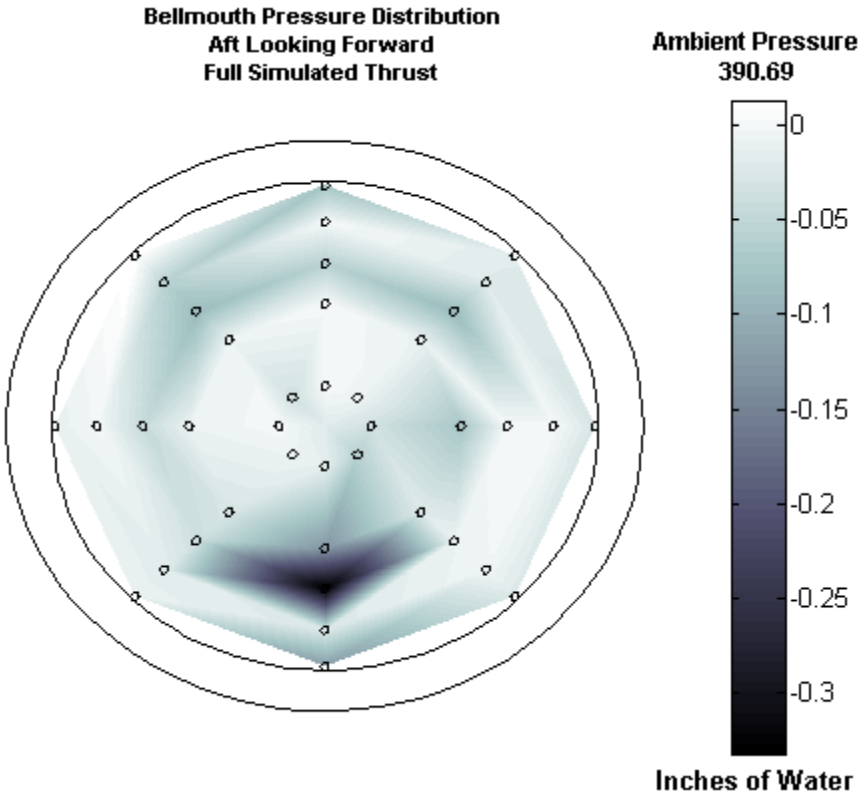

Figure 24: Artificial Vortex Capture (Weak)

Both Figure 24 and Figure 25 illustrate how unsteady these vortices can be. In the figure above, areas of low pressure can be seen throughout the face of the inlet. This is likely due to the vortex moving about the inlet, influencing pressure drops at various rakes as it travels. Because the vortex generator is located just beneath rake five, the vortex is most likely going to be ingested at the bottom of the engine inlet. In fact, a majority of runs where a vortex was captured indicated its presence on the bottom rake. However, in one particular run, as seen in the figure below, the vortex had actually swept upwards, causing a significant pressure drop on rake eight.

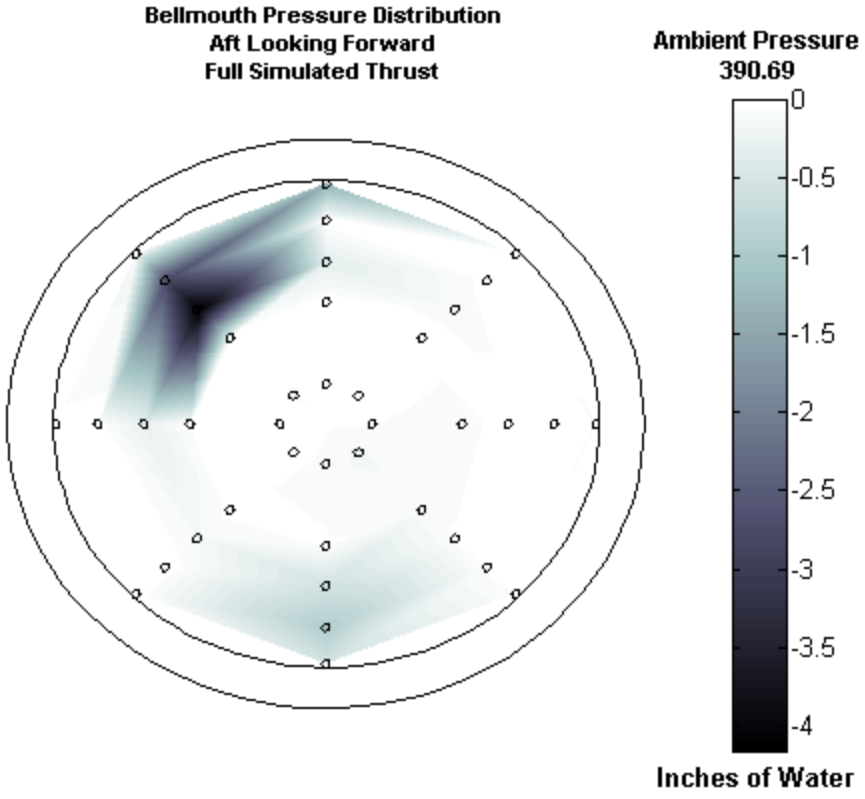

Figure 25: Vortex Unsteadiness Example

The inlet distortion seen above is 1.07% overall, over three times the acceptable distortion as defined by the SAE.

In order to understand how the inlet distortion compares to a naturally occurring vortex, the engine was run without the vortex generator running until a natural vortex was observed.

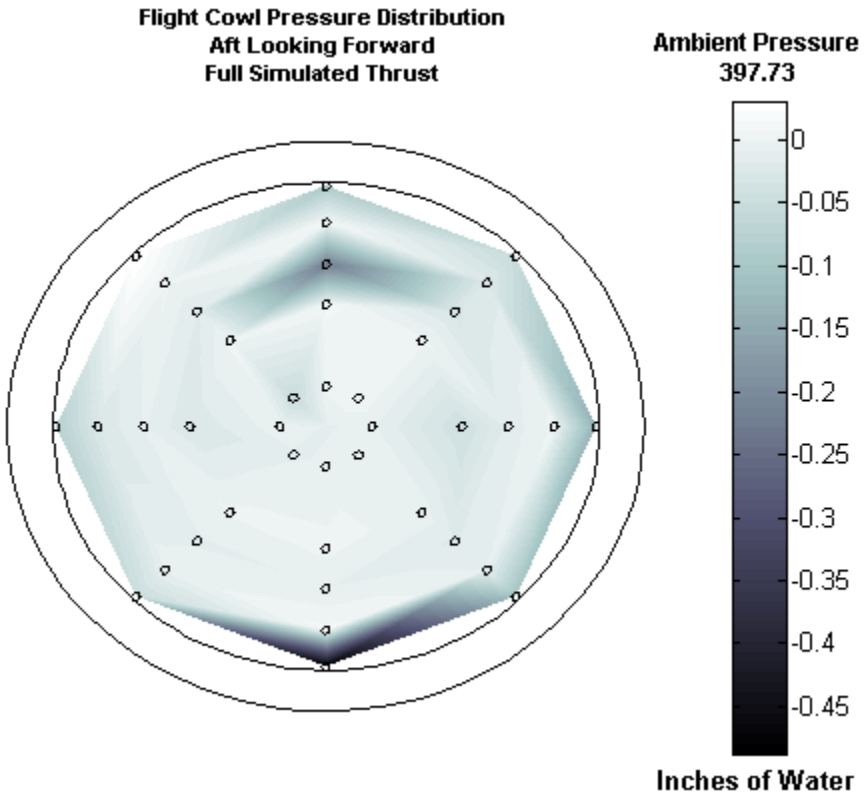

Figure 26: Naturally Occurring Vortex

As seen above in Figure 26, the naturally occurring vortex has a very similar pressure distribution as seen in Figure 23 and Figure 24. The engine was run at simulated full thrust and the overall bellmouth distortion was 0.13%. Additionally, there are pockets of lower pressure in the top half of the engine inlet that indicate the unsteady nature of the vortex. One main difference between the natural and forced vortex is that the natural vortex was ingested into the ring closest to the inside edge of engine. This could just be the result of unsteadiness. However, another possible scenario is that the artificial vortex is being forced up into the engine, potentially causing the vortex to be ingested nearer to the engine centerline than a naturally

occurring vortex. A naturally occurring vortex will be ingested in the boundary layer, closer to the edge of the engine. This is exactly what is seen above in Figure 26.

4.1.1 Transient Pressure Results

The LabVIEWcode was then updated to provide transient read-outs of the pressures measured in the engine inlet. Prior to this, the code averaged the pressure values over a five-second time interval to obtain the engine inlet distortion. If a vortex passed over a rake, the averaged data would surely have been able to show it; however, viewing the pressure values in real time makes the vortex easier to identify. First, the engine was run over the ground plane without the vortex generator running. Below in Figure 27, the instantaneous pressure measurements inside the engine inlet can be seen for an engine run without the vortex generator operating. Only the ports on rake five are shown in the figure as this is the most likely location for a vortex to appear. As expected, there are several spikes where the pressure drops due to naturally forming vortices. That is, the vortex is forming, moving, and disappearing during the entirety of the engine run. Ring four appears to be affected most consistently, although the effects on ring five are much clearer near the 25 second mark.

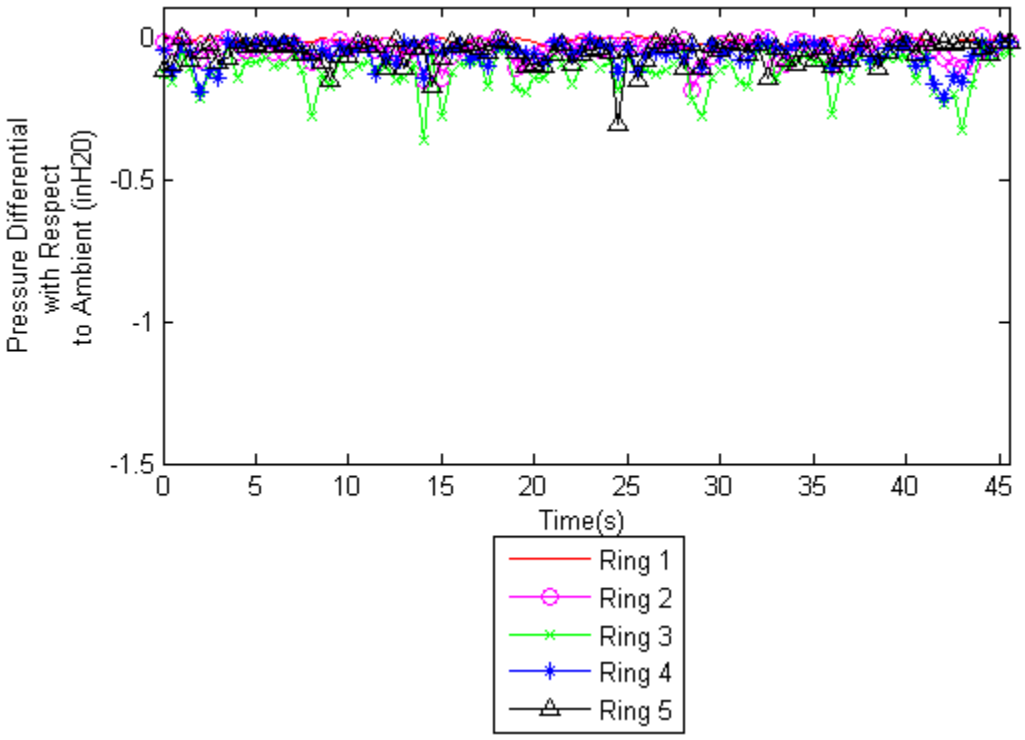

Figure 27: P7PT5 without Vortex Generator

The engine was run again with the vortex generator in full operation. These results can be seen in Figure 28. In this run, the vortex is constantly being forced. That is, a vortex will be ingested into the engine at all times. Interestingly, ring four again seems to be affected most consistently. Ring five was also hit one time, although the pressure drop induced was much more significant than before. To reiterate, this does not necessarily conclude that the artificial vortex is "stronger" than the naturally occurring vortex. It is more likely that in this experimental run, the vortex actually passed much more closely to ring five than previously, causing its effects to be seen much more clearly. Also, notice that many times when there is a drop in pressure in ring four, there are simultaneous spikes in other rings. This is especially noticeable near the 26 second mark. Again, this is due to a vortex coming close enough to the entire rake that multiple rings are being affected by its presence.

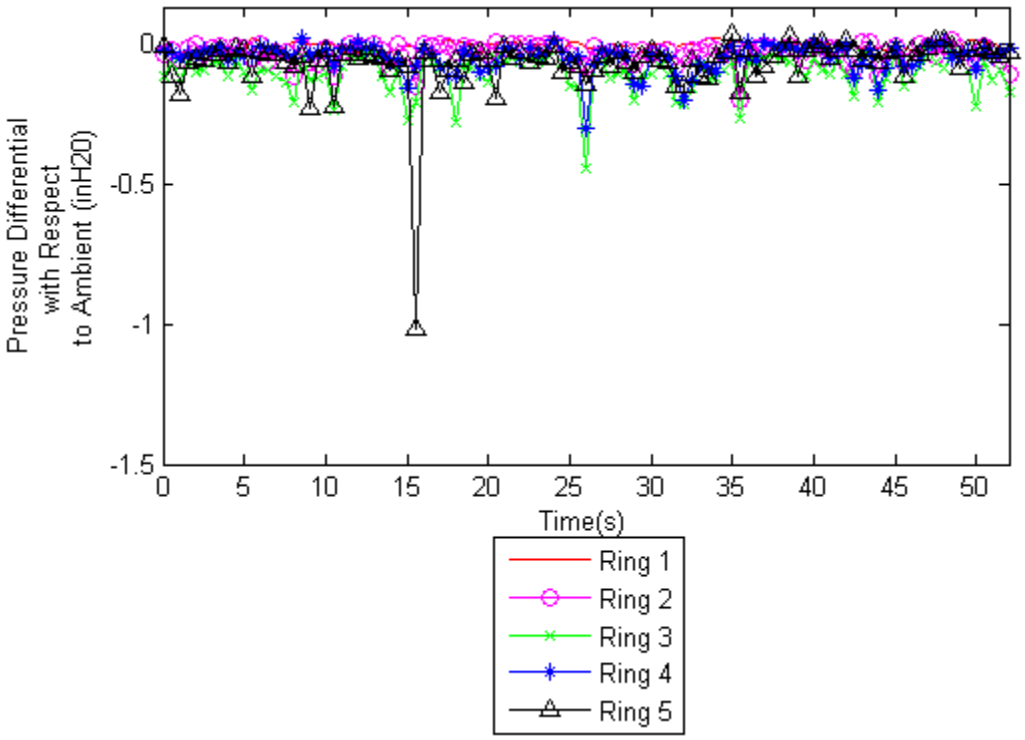

Figure 28: P7PT5 with Vortex Generator at Mass Fraction 6.82

These two prior figures indicate that the vortex generator does indeed produce effects on the engine inlet in the same way that a naturally occurring vortex might.

P7PT5RG5 was then isolated from the other rings and plotted on its own. This ring was especially of interest due to the fact that it is located at the very bottom of the engine, or in the boundary layer. In the following figures, the "baseline" simply refers to engine runs absent the vortex generator and is shown in blue. The red line indicates values recorded while the vortex generator is running.

Figure 29 is an example of the extreme unsteadiness of a vortex in the boundary layer. Again, the vortex generator forces a vortex to be present, whereas the blue line does not.

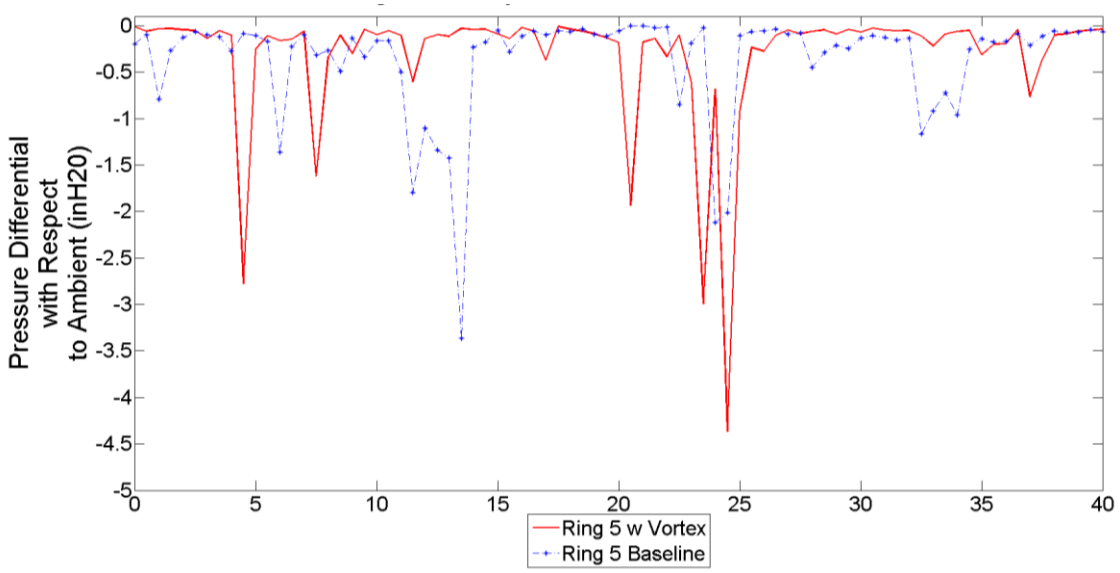

Figure 29: Sweeping Vortex Example

In each case, there are random drops in pressure that occur in ring five. Each of these spikes is an indication of the vortex passing near enough to the port that a pressure drop is induced. This is another example of how the vortex generator can accurately imitate the distortion seen in an engine inlet as caused by a naturally occurring vortex.

The relationship between mass fraction and inlet distortion was further investigated using the transient LabVIEW code. Pressure fluctuations in P7PT5RG5 were analyzed as this is the most probably location of vortex ingestion. Unfortunately, with the new LabVIEW code, exact inlet distortions could not be calculated. Therefore, the trends associated with changes in mass fraction can only be inferred based on the effects seen inside the engine inlet. Recall that a smaller mass fraction results from higher mass flow through the vortex generator. Each of the following three figures will have two plots. The solid and starred lines are with and without the vortex generator in operation, respectively. A run corresponding to a mass fraction of approximately 100 can be seen below in Figure 30. The vortex generator was run with tangential flow only; i.e. the axial pressure was set to zero.

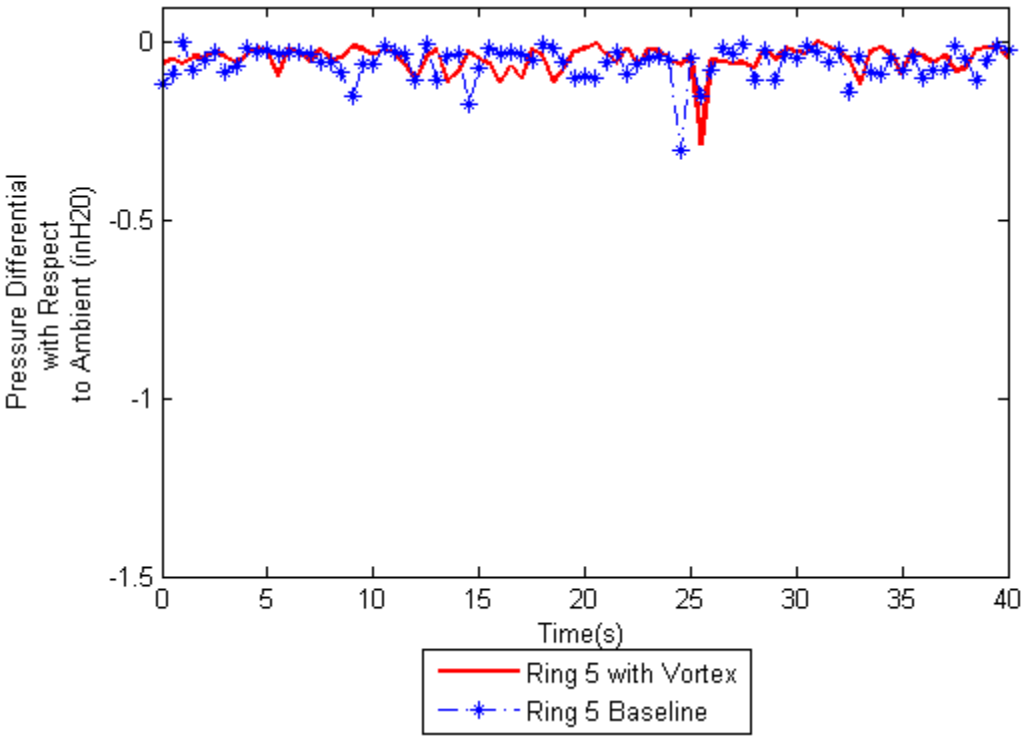

Figure 30: Ring Five Average with Mass Fraction of 100

In Figure 31, the mass fraction decreased to approximately seven as the axial pressure was set to a non-zero value and the plenum pressure remained unchanged. There is a slight increase in magnitude of the pressure spikes seen in this bottom port. A further increase in mass flow through the generator can be seen in Figure 32 where the mass fraction drops to approximately five. Again, the magnitude in pressure drop below ambient increased.

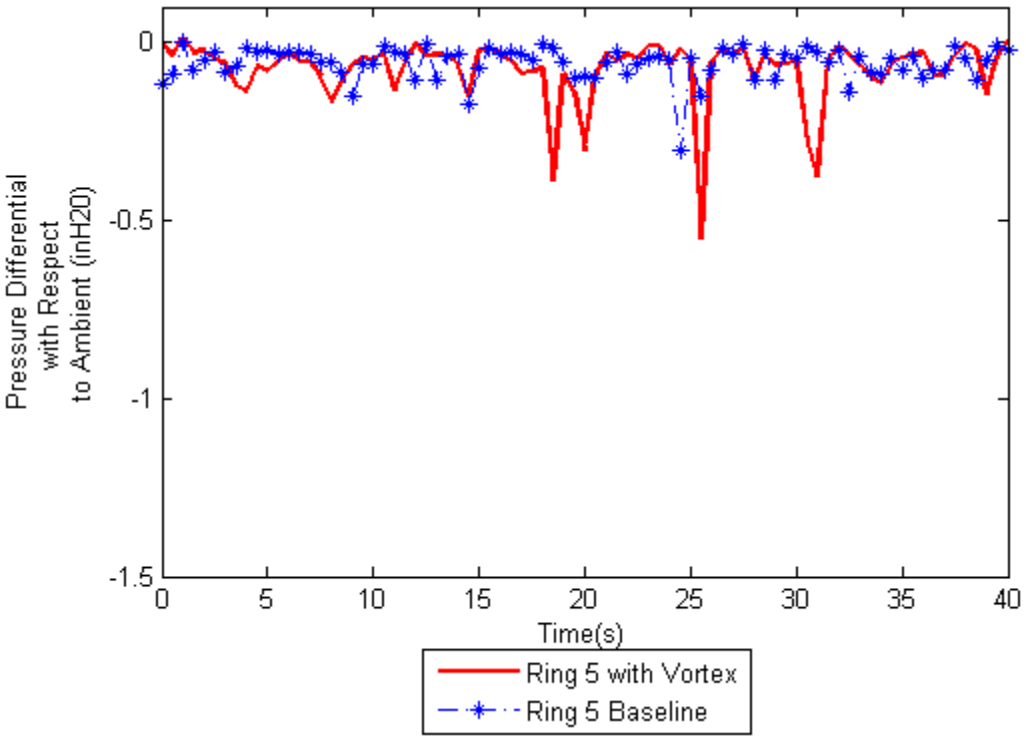

Figure 31: Ring Five with Mass Fraction of Seven

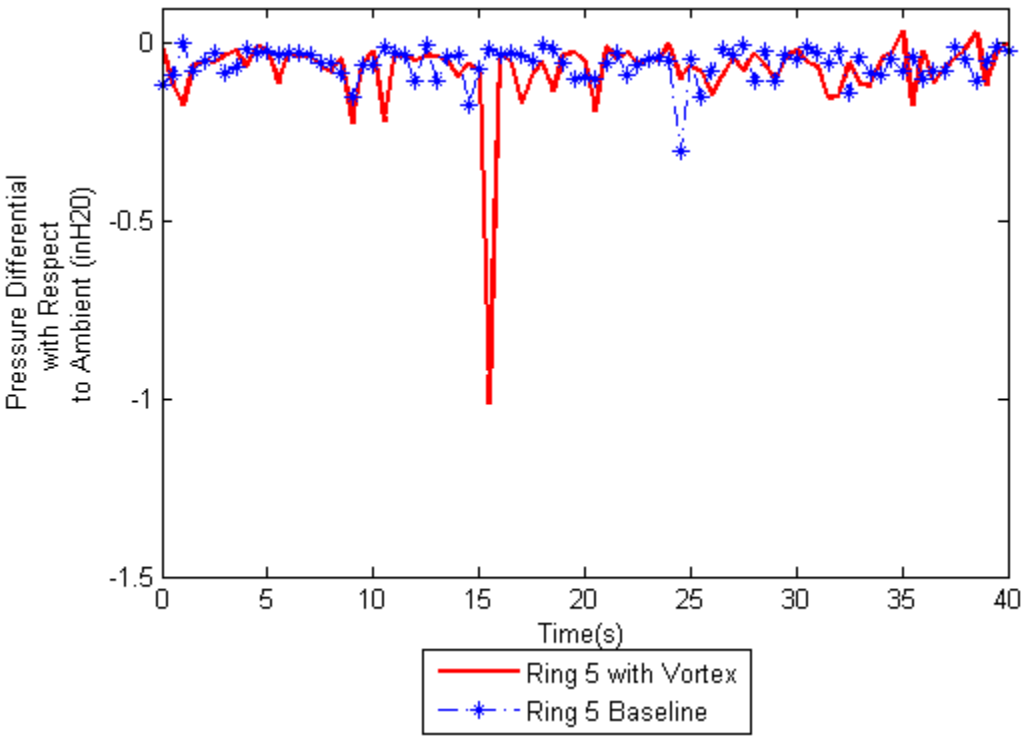

Figure 32: Ring Five with Mass Fraction of Five

Because we do not have exact inlet distortion calculations, only inferences can be made. From this pattern, it would be logical to assume that the inlet distortion would increase with a reduction in mass fraction. Rather, the mass flow exiting the vortex generator and the inlet distortion seen in the inlet of the engine simulator appear to be directly related.

4.2 Vortex Effects on Static Pressure

Along the bottom edge of the engine simulator, six static pressure ports are located just in front of rake five. The first static port is one-eighth of an inch from the leading edge, with 0.25 inch spacing for each consecutive port. The spacing between the fifth and sixth port grows to 0.75 inches, placing the sixth static port at 1.875 inches from the leading edge.

The engine was run without the vortex generator operating in a free field environment in order to obtain static pressure measurements under normal operating conditions. This data was then compared to data obtained during a time when the vortex generator was running at a mass fraction of 6.82 and a vortex was evident in the captured data.

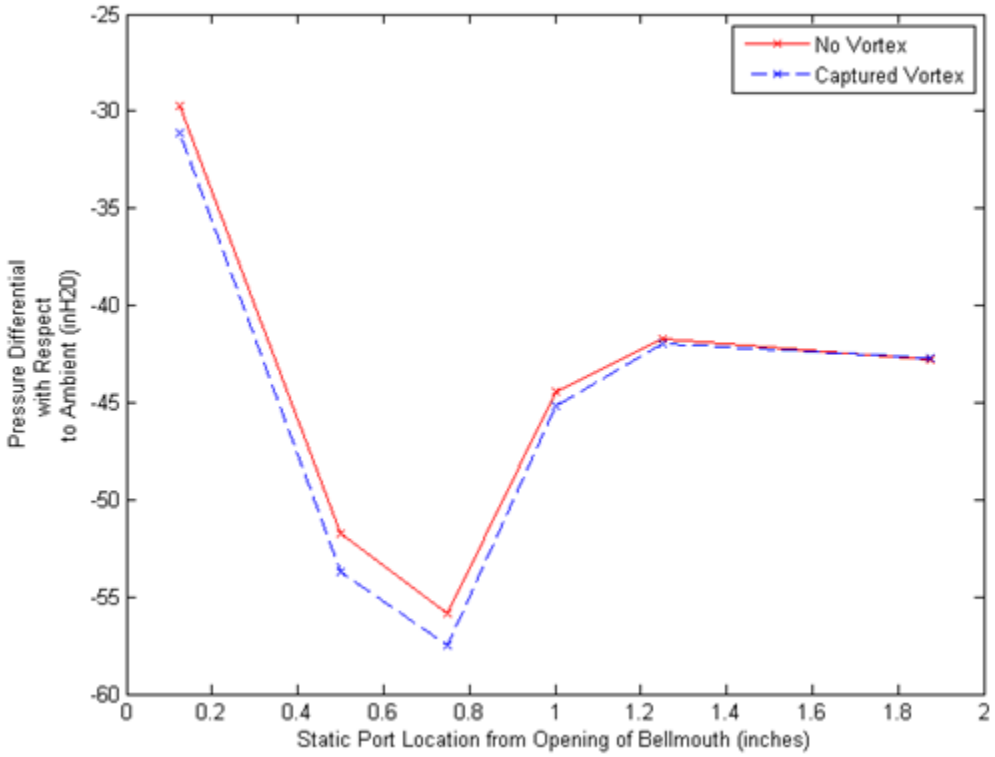

Figure 33: Static Pressure Changes at Full Thrust Simulation

In Figure 33, the static pressure is reduced from the inlet to approximately one inch downstream. This decrease in pressure is due to an increase in flow velocity in the boundary layer. As the vortex is ingested, it is pulling on the fluid in the boundary layer. Because it is directly proportional to velocity, the Reynolds number will also increase. A larger Reynolds number is indicative of a boundary layer that will transition to turbulent flow more quickly than before. It is possible that boundary layer separation will also occur more quickly. A separated boundary layer will adversely affect the performance of the engine and should be avoided.

Chapter V:
Conclusions and Future Work

The goal of this research project was to design and build a vortex generator that could consistently provide a vortex to an engine simulator and yield similar patterns in engine distortion as seen by a naturally occurring vortex. Vortex effects on static pressure inside the engine simulator were also analyzed.

A vortex generator was designed and fabricated using a similar technique as a previous research project at the AARL. The generator was validated both visually and experimentally. Further analysis revealed that a vortex has a significant effect on the boundary later in the bellmouth, causing an increase in flow velocity and decrease in static pressure.

In future work this author would suggest further refinement in the vortex generator. Although it did provide a vortex, the physical properties of the vortex, such as vorticity, are unknown and an attempt should be made to quantify them. From here, adjustments can be more easily made to better simulate a naturally occurring vortex.

References

1. “Vortex.” *Wikipedia” The Free Encyclopedia.* Wikimedia Foundation, Inc., (24 Februaary 2016. Web. (03 March 2016).

2. Trapp, Luís Gustavo, and Roberto Da Motta Girardi. "Crosswind Effects on Engine Inlets: The Inlet Vortex." *Journal of Aircraft* 47.2 (2010): 577-90.

3. Bowyer, E.p., and V.v. Krylov. "Damping of Flexural Vibrations in Turbofan Blades Using the Acoustic Black Hole Effect." *Applied Acoustics* 76 (2014): 359-65. Web.

4. Horvath, Nathan Rosendo. *Inlet Vortex Formation Under Crosswind Conditions.* Master of Science Thesis. Worcester Polytechnic Institute, 2013.

5. Colehour, J. L., and Farquhar, B. W., “Inlet Vortex,” *Journal of Aircraft*, Vol. 8, No. 1, January
1971, pp. 39-43.

6. Ho, W., *A Consolidated Study Regarding the Formation of the Aero-Inlet Vortex.* Advances in Intelligent Modelling and Simulation, 2012: p. 345-364.

7. Mitchell, Glenn A. *Effect of Inlet Ingestion of a Wing Tip Vortex on Compressor Face Clow and Turbojet Stall Margin.* NASA TM X-3246 Report, 1975.

8. Freuler, Richard Jeffrey. *An Investigation of Jet Engine Test Cell Aerodynamics by Means of Scale Model Test Studies with Comparison to Full Scale Test Results.* Diss. The Ohio State University, 1991.

9. Allenstein, Jacob T. *An Investigation in Gold-Plating Scaled Turbofan Engine Simulators through Means of Aerodynamic and Load Cell Thrust Measurements with Comparison to Full-Scale Engine Results.* Master of Science Thesis. The Ohio State University, 2013.

10. Montgomery, Kirk. *The design, instrumentation, and operation of a free field test stand for a scale model turbofan simulator.* Master or Science Thesis. The Ohio State University, 1990.

11. *Measurement Uncertainty: Instruments and Apparatus.* ANSI/ASME PTC 19.1 – 1985. American Society of Mechanical Engineers, Reaffirmed 1990.

12. S-16 Turbine Engine Inlet Flow Distortion Committee. *Gas Turbine Engine Inlet Flow Distortion Guidelines*. Tech. No. SAE ARP 1420b. SAE International.